ACS OMEGA

http://pubs.acs.org/journal/acsodf

Article

SiN_x/Cu Spectral Beam Splitting Films for Hybrid Photovoltaic and Concentrating Solar Thermal Systems

Xin Zhang, Dongqiang Lei,* Bo Zhang, Pan Yao, and Zhifeng Wang

Cite This: *ACS Omega* 2021, 6, 21709−21718

Read Online

ACCESS | Metrics & More | Article Recommendations

ABSTRACT: Spectral beam splitting (SBS) films are crucial for the development of hybrid systems based on photovoltaic (PV) and concentrating solar thermal (CST) technologies. In this study, a novel double-layer SiN_x/Cu SBS film was prepared via magnetron sputtering. This film was developed based on the linear Fresnel solar thermal technology used in PV/CST hybrid systems. The as-deposited film exhibited superior SBS properties, with a high transmittance of 72.9% and a reflectance of 89.7%. To optimize the optical properties, the thicknesses of the metal and SiN_x layers were precisely controlled. The optimal thicknesses of the Cu and SiN_x layers were determined to be 17 and 67 nm, respectively. Furthermore, the thermal stability of the SBS film was evaluated. When annealed at 50 °C, the surface of the SBS film became more uniform and smooth, and with increasing annealing time, the film became denser. No strong diffraction peaks of Cu were observed in the X-ray diffraction patterns because of the low content and poor crystallization of Cu. Atomic force microscopy investigations revealed the formation of a textured surface and a decrease in the root-mean-square roughness with an increase in the annealing time from 0 to 360 h. As a key component with considerable application potential in PV/CST hybrid systems, SBS films are currently an important research topic.

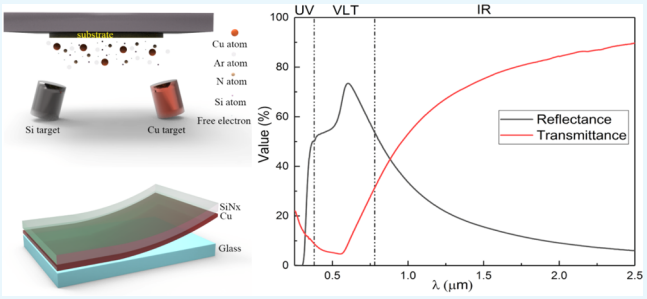

1. INTRODUCTION

The global energy crisis caused by the depletion of non-renewable resources and the serious environmental issues caused by the use of fossil fuels have led to an increase in the demand for renewable energy sources. In the current era of carbon neutrality, renewable energy technologies have attracted worldwide attention.[1] The development and application of solar energy technologies have been actively promoted by various countries owing to their eco-friendliness and multiroute development, as well as flexible access to the abundant solar energy.[2,3] There are two main technologies for harvesting solar energy, concentrating solar thermal (CST) and photovoltaic (PV), which facilitate the direct conversion of solar energy into heat and electricity, respectively.[4−6] Although a CST system can convert the full solar spectrum into thermal energy, its efficiency in converting solar radiation into power after concentration is relatively low. This drawback has limited the development of CST systems.[7] PV systems offer strong spectral selection characteristics; they generate electricity only in the visible to near-infrared (NIR) regions, and the rest of the spectral range is either lost or absorbed by the PV cell to generate heat.[8] Therefore, to maximize the utilization of solar energy, a hybrid PV/CST system based on spectral beam splitting (SBS) has been proposed by numerous researchers. PV/CST hybrid systems with low-cost SBS films are simple and compact. SBS films, which are the most crucial components of such hybrid systems, must offer outstanding solar transmittance in the wavelength range of 300−1100 nm and maximized solar reflectance in the wavelength range of 1100−2500 nm.[9−11]

Numerous studies have focused on the development of SBS films, which can be classified into two types: (i) interlaced high-refractive index and low-refractive index dielectric materials and (ii) metal/dielectric materials. Such films divide the solar spectrum into two parts: one in the wavelength range of 400−1100 nm for PV conversion and the other in the wavelength range of 1100−2500 nm for photothermal conversion, as illustrated in Figure 1. For example, Liang et al.[12] prepared a SiO_2/TiO_2 multilayer SBS film with a high average reflectance ($\rho \geq 96.8\%$) at 300−1100 nm and a high average transmittance ($\tau \geq 85\%$) at 1100−2500 nm. Other optical materials used for SBS films include Ge, Nb_2O_3, Ta_2O_5, and Na_3AlF_6. Further, Wang et al.[13] designed a multilayer SBS film consisting of 13 layers and reported an average

Received: June 17, 2021
Accepted: August 4, 2021
Published: August 15, 2021

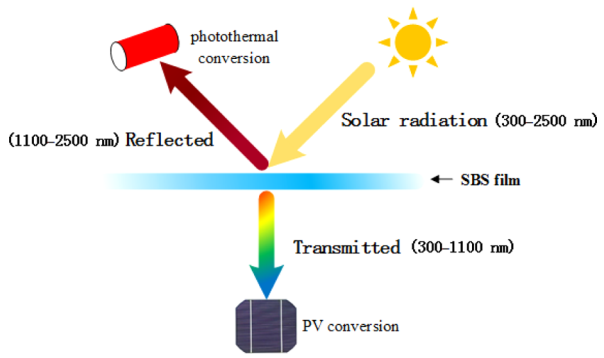

Figure 1. Schematic of a hybrid system based on a spectral splitting film.

transmittance of 72.1% and a reflectance of 27.9% in the wavelength range of 250−2500 nm. In the past decade, various tandem multilayer films, such as SiO_2/TiO_2,[14] Nb_2O_5/SiO_2,[15,16] SiO_2/Ta_2O_5,[17] Ge/SiO_2,[18] SiN_x/SiO_2,[19] and $Ge/Nb_2O_3/Na_3AlF_6$,[10] have been utilized in hybrid CPV/ST or PV/CST systems. However, such coatings require strict control of the film thickness and the superimposition of multiple layers of various materials, which increase the complexity of processing SBS films. Therefore, single metal/dielectric coatings with intrinsic spectral selectivity have attracted considerable attention owing to their advantages such as simple processing, fewer film layers, and ease of control over the film thickness.

Currently, metal layers are being used as highly reflective layers for the infrared (IR) spectral range. However, there are only a few reports on their application in SBS films. Thin layers of Ag, Au, Cu, and other metals transmit visible and NIR wavelengths of the solar spectrum and reflect mid-IR and IR wavelengths.[20] Wamg et al.[21] designed a Ag−Cu alloy film with high reflectance and reported that the reflectance decreased as the annealing temperature exceeded 100 °C. Li et al.[22] fabricated a coating of aluminum-doped zinc oxide (AZO)/Ag/AZO(40/12/40 nm) with an optical transmittance of >80% in the region of 380−780 nm. A 7 nm thick Cu layer sandwiched between Ga-doped ZnO films exhibited an average transmittance of >70% in the visible-light range.[23] To improve the transmittance, an anti-reflection (AR) layer of a dielectric material, such as AlN,[24] Al_2O_3,[25] SiO_2,[26] SiON,[27] or SiN_x,[28] was added on the metal layer.

In this work, we prepared a double-layer SBS film of SiN_x/Cu on glass by magnetron sputtering. The optimized SBS film obtained by varying the process parameters of magnetron sputtering, such as the gas flow rate, sputtering power density, and deposition time, exhibited superior SBS characteristics. The reflectance (ρ) and transmittance (τ) of the SiN_x/Cu SBS films were investigated using a Cary 7000 UV/Vis/NIR spectrophotometer. Moreover, their structure and thermal stability were studied in detail via field-emission scanning electron microscopy, energy-dispersive X-ray spectroscopy (EDS), atomic force microscopy (AFM), and X-ray diffraction (XRD). The double-layer SBS film showed good optical performance and thermal stability and is expected to broaden the application prospects of PV/CST hybrid systems.

2. RESULTS AND DISCUSSION

The double-layer SiN_x/Cu film on glass exhibited excellent SBS characteristics, with an average transmittance of 54.8% in the wavelength range of 380−1100 nm and a reflectance of 67.7% in the wavelength ranges of 300−380 and 1100−2500 nm. The transmittance and reflectance of a film depend on the material type, surface features, structure, and roughness. The thickness of each layer was determined by cross-sectional SEM studies of the SiN_x/Cu SBS films. To further analyze the optical performance of the SiN_x/Cu SBS film, the effects of the thicknesses of the SiN_x and Cu layers as well as annealing conditions on the optical properties were examined in detail.

2.1. Structural Analysis. The microstructure of the SiN_x/Cu SBS film was investigated to determine its potential influence on the transmission and reflection characteristics. The schematic of the sputtering process in Figure 2a shows the substrate, targets, and working atoms. Argon (Ar) ions were

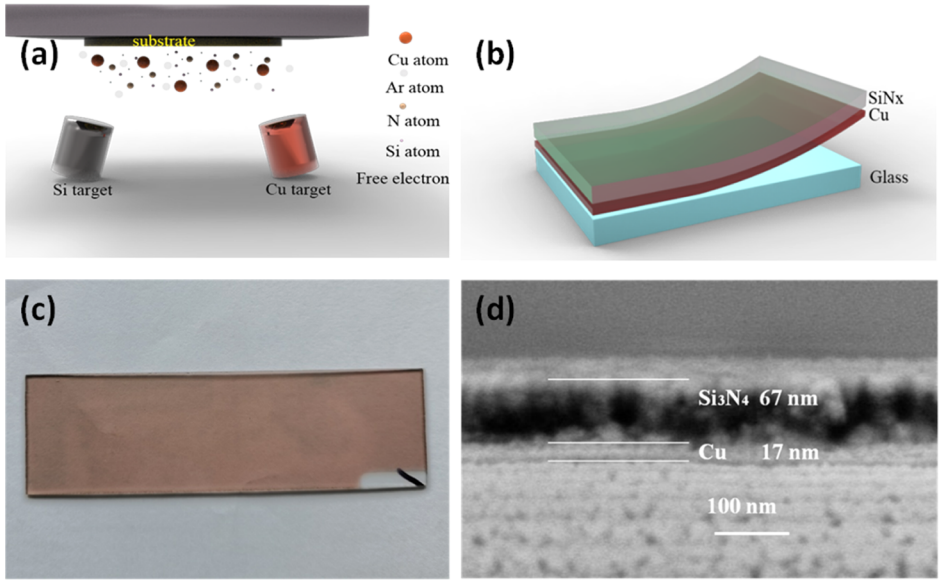

Figure 2. (a) Pictorial representation of the magnetron sputtering process, (b) schematic of the SiN_x/Cu SBS film deposited on glass, (c) photograph of the SiNx/Cu SBS film, and (d) cross-sectional morphology of the SiN_x/Cu SBS film.

https://doi.org/10.1021/acsomega.1c03178
ACS Omega 2021, 6, 21709−21718

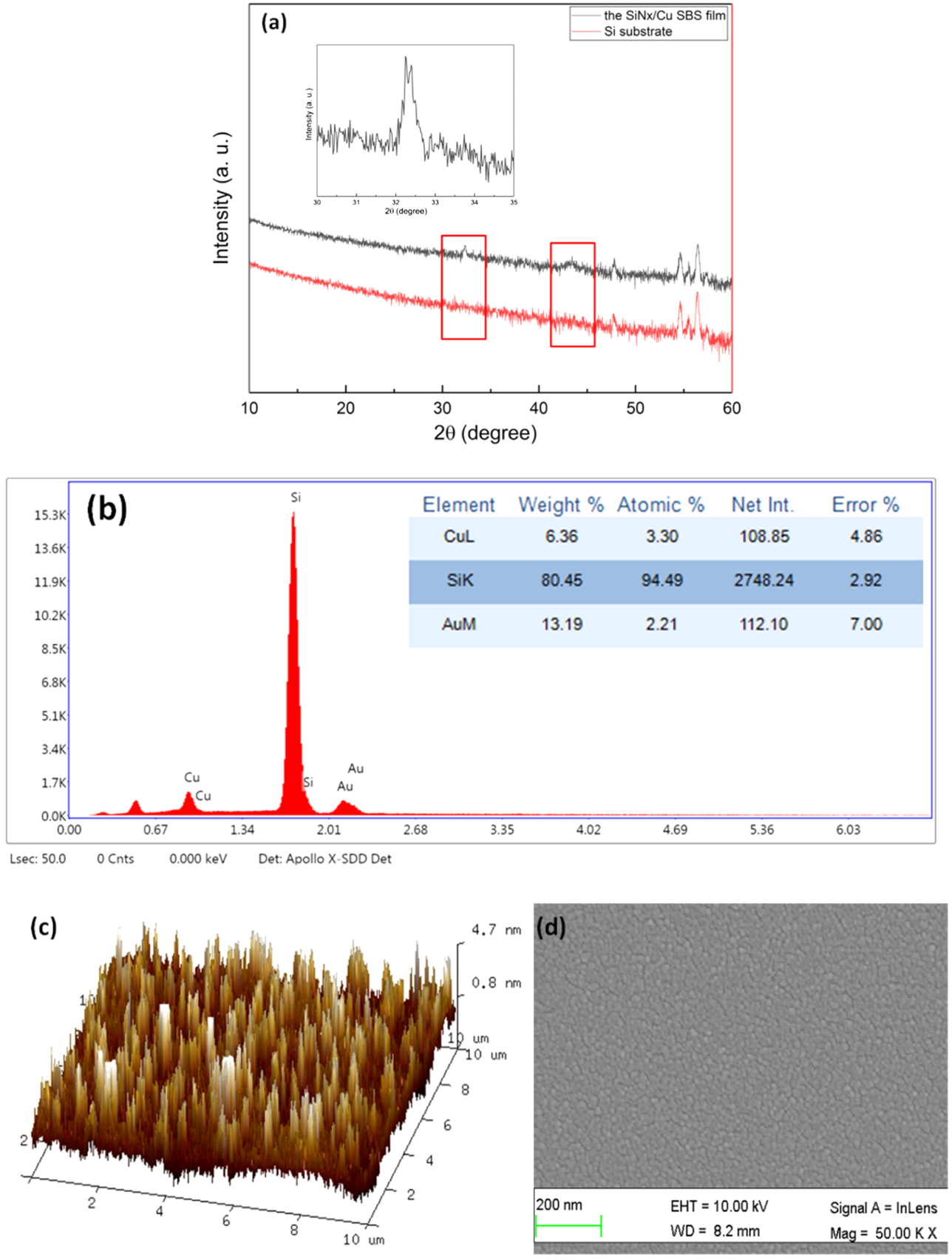

Figure 3. (a) XRD pattern, (b) EDS profile, (c) 3D AFM image, and (d) SEM image of a SiN_x/Cu SBS film.

generated by glow discharge in a vacuum environment and bombarded onto the target, and the ejected target material was deposited on the substrate to form a film. Figure 2b shows a schematic of the SBS film. The Cu layer was deposited directly

https://doi.org/10.1021/acsomega.1c03178
ACS Omega 2021, 6, 21709−21718

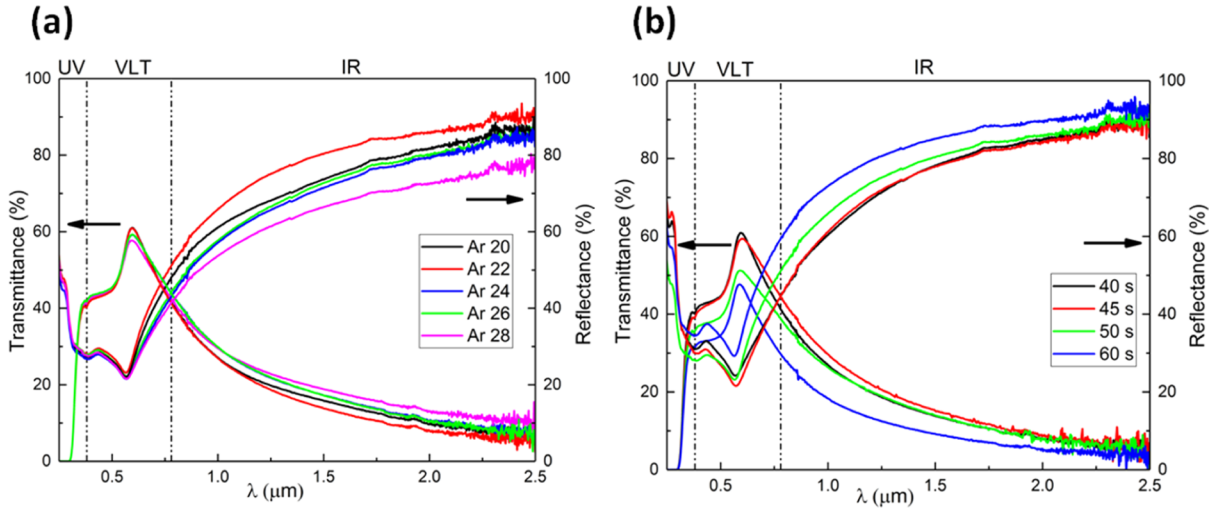

Figure 4. Transmittance and reflectance spectra of the single layers of Cu obtained at (a) different Ar flow rates and (b) different sputtering times.

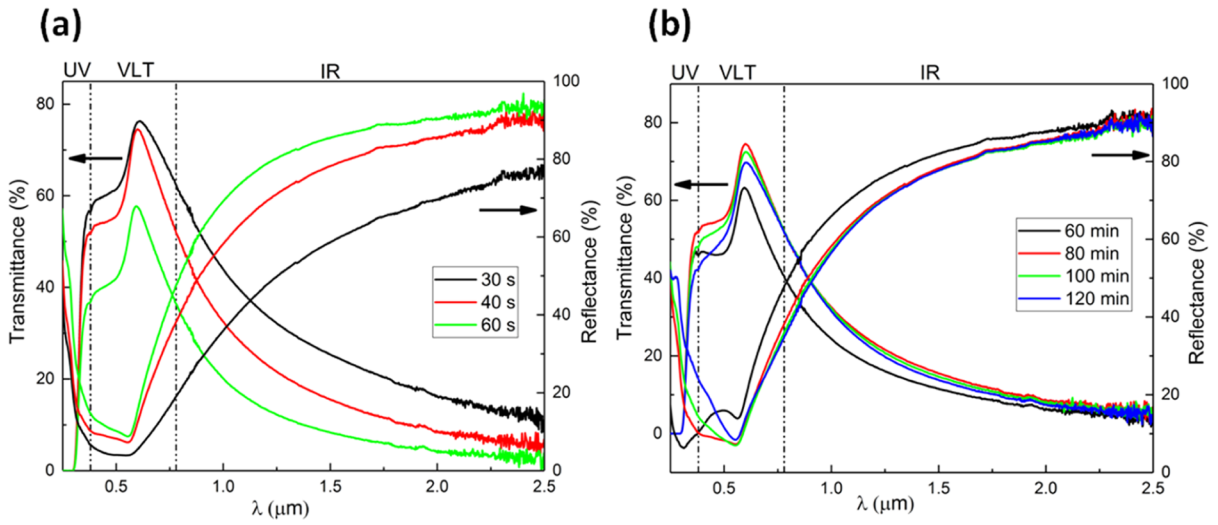

Figure 5. Transmittance and reflectance spectra of (a) Cu layer sputter-deposited on the SiN_x layer for different durations and (b) SiN_x layer sputter-deposited on the Cu layer for different durations.

on the BK7 glass substrate. Subsequently, the SiN_x layer was deposited on the optimized Cu layer. Figure 2c shows a photograph of the reddish-brown SiN_x/Cu solar SBS film obtained by magnetron sputtering. The Cu layer is reddish-brown, while the SiN_x layer is transparent. Figure 2d presents a cross-sectional SEM image of the SiN_x/Cu SBS film deposited on a Si substrate. The image shows the two distinct layers of the SBS coating and the columnar structure of the SiN_x layer. The thicknesses of the Cu and SiN_x layers were measured to be ~17 and 67 nm, respectively.

Figure 3a shows the XRD pattern of the SiN_x/Cu solar SBS film on Si, along with that of the Si substrate. The XRD pattern of the sample is similar to that of the substrate, with minor differences in the 2θ range of 30 to 35°. The diffraction pattern of the SiN_x/Cu SBS film shows a weak peak at 32.3°, which is enlarged in the inset of Figure 3a. This low-intensity peak corresponds to the (110) plane of Cu_2O and indicates that the Cu_2O phase was formed in the deposited film; similar results have been reported earlier.[29−31] Another broad and weak peak is also observed at ~45°, corresponding to the (200) plane of Cu_2O in the XRD pattern of the deposited film. No strong diffraction peaks of Cu are observed because of its low content and poor crystallization. This result also implies good dispersion of the very small Cu agglomerates on the surface of the Si substrate. The rest of the diffraction pattern shows broad amorphous features, with no peaks indicative of crystalline phases. Thus, the XRD pattern reveals the presence of a thin Cu layer and the amorphous nature of the SiN_x layer.

The microstructure and composition of the sample were further analyzed by EDS. Figure 3b shows the chemical composition of the SiN_x/Cu SBS film determined by microanalysis. Gold was spray-coated on the SiN_x/Cu SBS film sample to successfully perform the EDS analysis. The results indicate that the coating consists of silicon and copper. The silicon signal mainly originated from the Si substrate on which the SiN_x/Cu SBS film was deposited.

Figure 3c shows a three-dimensional (3D) AFM image of the SiN_x/Cu SBS film with a columnar structure. The film has a textured surface with a root-mean-square (rms) roughness of 1.06 nm (as determined using NanoScope Analysis software). The uniform, smooth, and dense surface of the SiN_x/Cu SBS film is evident in the SEM image in Figure 3d. Many gold particles (used for staining the sample) can be observed on the surface of the SiN_x/Cu SBS film, and there is no apparent

https://doi.org/10.1021/acsomega.1c03178
ACS Omega 2021, 6, 21709−21718

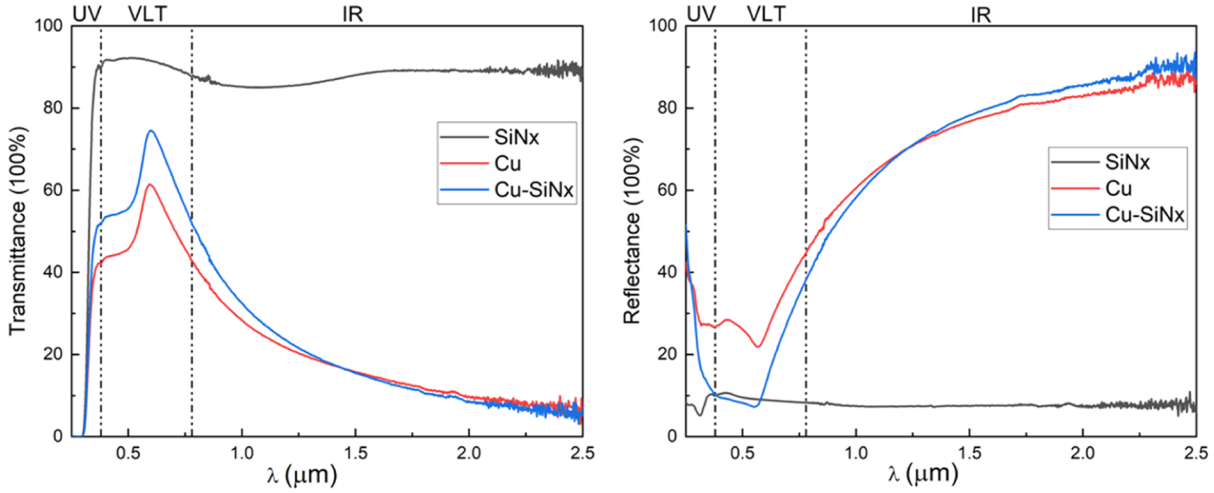

Figure 6. Variation in the transmittance and reflectance spectra of Cu, SiN_x, and Cu/SiN_x films.

particle agglomeration at the scale of 200 nm in the SEM images. The AFM and SEM images indicate the formation of a uniform and dense sample surface, which is important for maintaining superior stability under long annealing times and also for preventing oxidation upon exposure to air.

2.2. Optical Properties. *2.2.1. Optimization of the Cu Layer.* The Cu layer has high transmittance in the wavelength range of 300−1100 nm and high reflectance in the wavelength range of 1100−2500 nm, as shown in Figure 4. Figure 4a,b shows the transmittance and reflectance spectra of the single Cu layers recorded at different Ar flow rates and sputtering times, respectively. As the Ar flow rate increased, the maximum reflectance in the IR region and the transmittance in the visible region decreased, as shown in Figure 4a. However, the highest transmittance and reflectance were observed at an Ar flow rate of 22 sccm. To determine the effect of the layer thickness on the optical properties, the sputtering time of the Cu layer was varied between 40 and 60 s at the Ar flow rate of 22 sccm and a constant sputtering power. The highest transmittance and reflectance were achieved for the shortest sputtering time, as shown in Figure 4b. However, the Cu grains in the thinner Cu layer are known to agglomerate to form a discontinuous metal film, leading to severe light scattering.[32,33] After a series experiments, an Ar flow rate of 22 sccm and a sputtering time of 40 s were used as the optimal sputtering parameters for the Cu layer.

The Cu layer thickness significantly affects the transmittance of the double-layer SiN_x/Cu SBS films in the visible and NIR regions of the solar spectrum. Furthermore, the overall effect of the thickness of the Cu layer on the transmission and reflection spectra is evident from Figure 4b. Figure 5a shows the transmittance and reflectance spectra of the SiN_x/Cu SBS films for different thicknesses of the Cu layer. It is clear that an increase in the thickness of the Cu layer (the sputtering time of the SiN_x layer was maintained) led to a distinct increase in the reflectance in the wavelength range of 780−2500 nm and a decrease in the transmittance in the visible region. As the Cu layer thickness increased, the cutoff wavelength shifted to a lower value. Considering the maximum transmittance in the visible range and the maximum reflectance in the IR range, the sputtering time of 40 s was chosen to be optimum for depositing the Cu layer on the double-layer SiN_x/Cu SBS film.

2.2.2. Optimization of the SiN_x Layer. The thickness of the SiN_x layer significantly affects the reflectance of solar energy in the IR region. Figure 5b shows the transmittance and reflectance spectra of the SiN_x layer prepared at different thicknesses. Increasing the thickness of the SiN_x layer (the Cu layer thickness was maintained) led to a distinct increase in the transmittance in the visible region and a decrease in the reflectance in the wavelength range of 780−2500 nm. As the SiN_x layer thickness increased, the cutoff wavelength shifted to a higher value because of the improved effect of SiN_x as an AR layer. As the maximum transmittance in the visible range and the maximum reflectance in the IR range were not significantly reduced, a sputtering time of 80 min was chosen to be optimum for the deposition of the SiN_x layer.

2.2.3. Spectral Properties of the SiN_x/Cu SBS Film. According to the above results, the thicknesses of the Cu and SiN_x layers significantly influence the transmittance and reflectance of the SBS film, respectively. Hence, we compared the optical properties of the SBS films with different Cu and SiN_x thicknesses and selected the best-performing film to carry out further spectral analysis. The optimized film consisted of a 17 nm thick Cu layer and 67 nm thick SiN_x layer and exhibited a maximum transmittance of 72.9% and a maximum reflectance of 89.7%. Figure 6 shows the transmittance and reflectance spectra of the Cu, SiN_x, and Cu/SiN_x films. The single layer of Cu shows intrinsic SBS characteristics,[32,33] and the addition of the SiN_x layer improves the SBS characteristics owing to the decrease in the reflected light.[28] Thus, the double-layer SiN_x/Cu SBS film exhibits a high average transmittance (τ = 54.8%) in the wavelength range of 380−1100 nm and a high average reflectance (ρ = 67.7%) in the ranges of 300−380 and 1100−2500 nm.

2.3. Thermal Stability. Different cooling systems have been proposed to ensure that the operating temperature of silicon PV cells is maintained below 50 °C.[34] For the transmission of solar spectral wavelengths in the range of 300−1100 nm to the PV cell, the SiN_x/Cu SBS film was coated on the PV cell. Subsequently, the thermal stability of the SiN_x/Cu solar SBS films was evaluated to assess their operating lifetime at 50 °C, which is the maximum operating temperature of silicon PV cells. We analyzed the transmittance and reflectance spectra of the coatings annealed at 50 °C for different durations; the results are shown in Figure 7. In

https://doi.org/10.1021/acsomega.1c03178
ACS Omega 2021, 6, 21709−21718

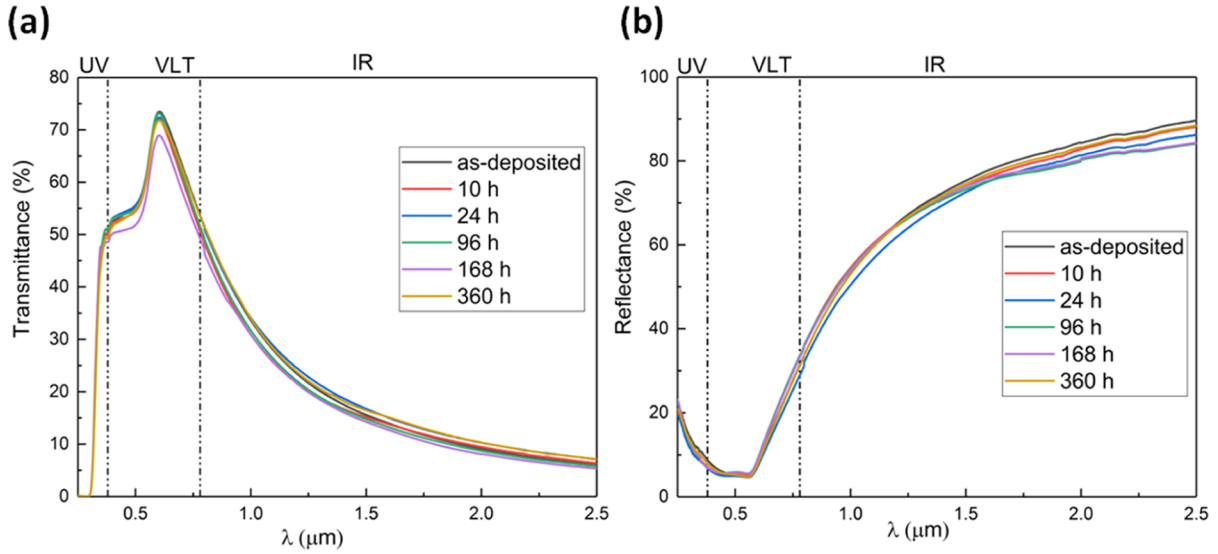

Figure 7. (a) Transmittance and (b) reflectance spectra of the SiN_x/Cu SBS coatings annealed at 50 °C for different durations.

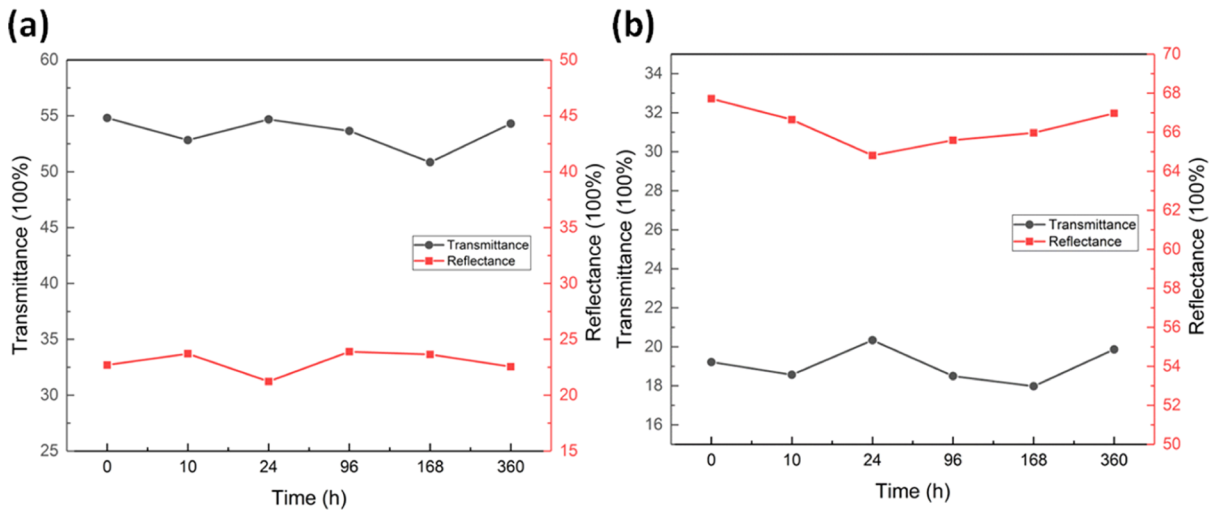

Figure 8. Variation in the (a) transmittance and (b) reflectance values of the coatings after annealing at 50 °C for different durations.

general, structural changes that occur due to long annealing times can lead to the attenuation of the optical properties of materials. The optical properties of the SiN_x/Cu solar SBS film prepared in this study did not change significantly after annealing. However, the maximum transmittance was reduced from 73.4% to 68.9% after annealing at 50 °C for 168 h and then increased to 71.8% after annealing for 360 h, as shown in Figure 7a. The maximum reflectance was reduced from 89.7% to 84.4% after annealing at 50 °C for 168 h and then increased to 88.5% after annealing for 360 h, as shown in Figure 7b. The variation of the optical efficiency of the film could be caused by the inter-diffusion of Cu. Figure 8 displays the average transmittance in the wavelength range of 380−1100 nm and the average reflectance in the wavelength ranges of 300−380 and 1100−2500 nm after annealing. We mainly focus on the trend of the average transmittance in the 380−1100 nm range (black curve) and the average reflectance in the 1100−2500 nm range (red curve) in Figure 8a,b, respectively. The transmittance and reflectance spectra fluctuate, rather than showing a continuous monotonic trend with a long measurement time. As the annealing time increased, the average transmittance of the film initially decreased and then increased after 168 h of annealing, as shown in Figure 8a. Evidently, the average reflectance of the SiN_x/Cu solar SBS films did not change considerably after annealing for 360 h, as shown in Figure 8b. These results suggest that the microstructure of the SiN_x/Cu solar SBS film is affected by the annealing duration, resulting in a decrease in the maximum transmittance and reflectance of the film.

SEM and AFM studies were performed to analyze the reasons for the minimal spectral changes of the SiN_x/Cu SBS films annealed at 50 °C for different durations. As shown in Figure 9a−f, the SiN_x/Cu SBS films maintained a uniform, smooth, and dense surface after annealing for different durations. The high-magnification SEM images clearly show the fine shape of the Ag particles (used for staining the sample) with uniform shapes and flat surfaces. This indicates that the surface morphology of the SiN_x/Cu SBS films did not change significantly after annealing at 50 °C for different durations. Figure 10a−f shows the 3D AFM images of the annealed SiN_x/Cu SBS films, which display the surface microstructure in detail. These are inconsistent with the two-dimensional SEM images. The AFM images show a porous film with gradually varying roughness; the rms roughness of the coatings

https://doi.org/10.1021/acsomega.1c03178
ACS Omega 2021, 6, 21709−21718

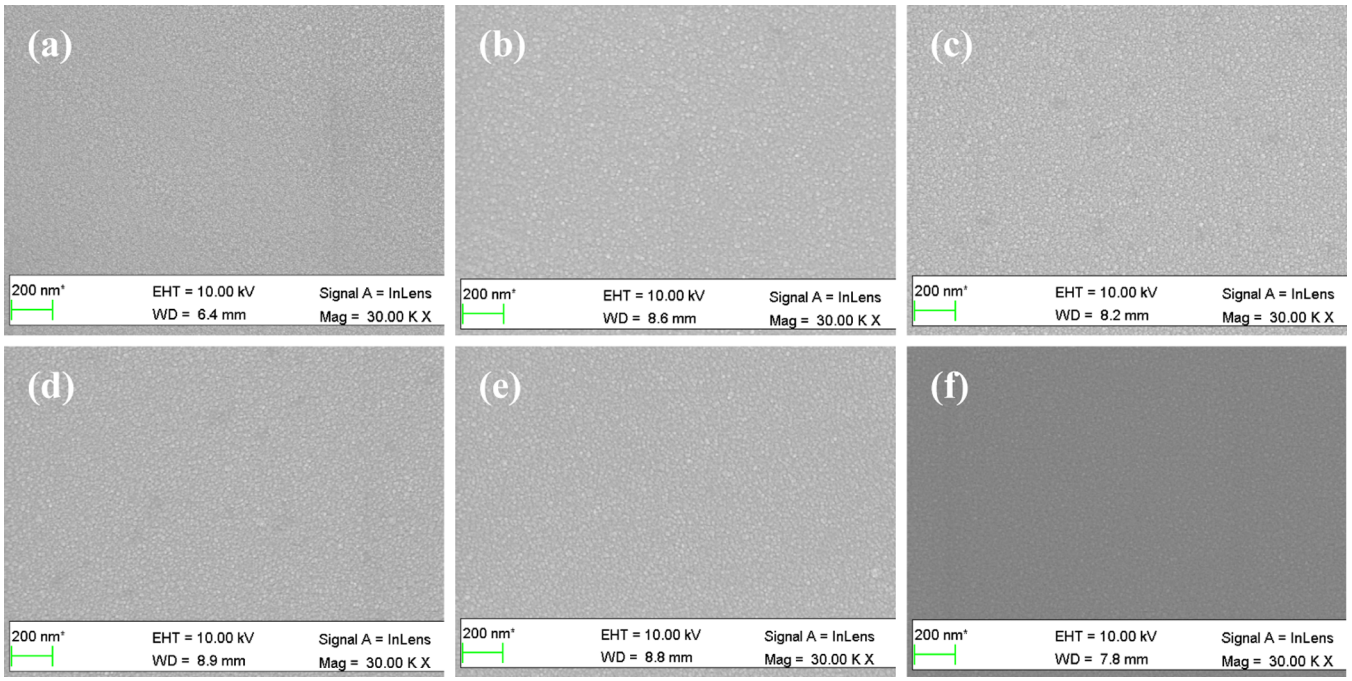

Figure 9. SEM images of the (a) as-deposited SiN_x/Cu solar SBS film and the SiN_x/Cu films annealed at 50 °C for (b) 10, (c) 24, (d) 96, (e) 168, and (f) 360 h.

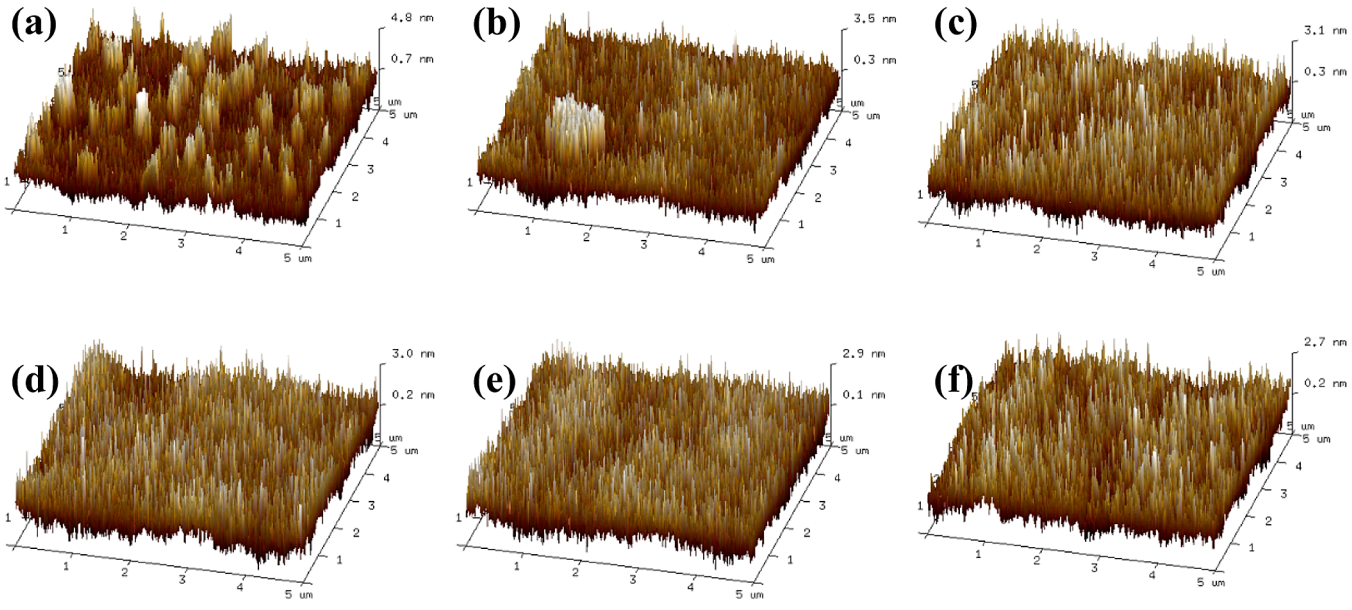

Figure 10. 3D AFM images of the (a) as-deposited SiN_x/Cu solar SBS film and SiN_x/Cu films annealed at 50 °C for (b) 10, (c) 24, (d) 96, (e) 168, and (f) 360 h.

decreased from 1.07 (as-deposited) to 0.84, 0.80, 0.81, 0.78, and 0.69 after annealing for 10, 24, 96, 168, and 360 h, respectively. The surface structure of the coatings became denser with increasing annealing time. The increased rms roughness enhances the diffuse reflectance and decreases the transmittance.[35] In brief, no significant changes were observed in the surface morphology of the coating, indicating excellent thermal stability of the films annealed at 50 °C for different durations (a high maximum transmittance of 71.8% and a reflectance of 88.5%). No diffusion of other atoms was observed in the coating at 50 °C. The long-term and high-temperature thermal stability of the SiN_x/Cu solar SBS film will be studied in the future.

3. CONCLUSIONS

A double-layer SBS film of SiN_x/Cu was prepared by magnetron sputtering. The SiN_x/Cu SBS film could divide the solar spectrum into two parts: one for PV conversion in the wavelength range of 300−1100 nm and the other for photothermal conversion in the wavelength range of 1100−2500 nm. To optimize the optical properties, the thicknesses of the metal and SiN_x layers were optimized by varying the sputtering power, sputtering time, Ar flow rate, and N_2 flow

https://doi.org/10.1021/acsomega.1c03178
ACS Omega 2021, 6, 21709−21718

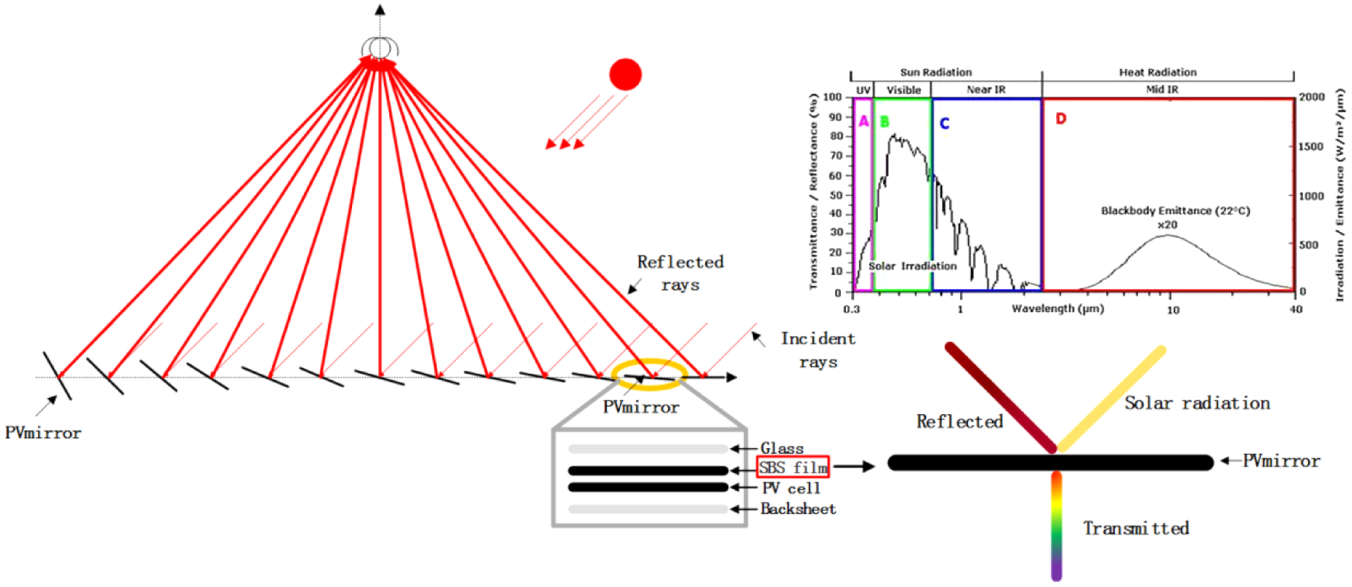

Figure 11. Schematic of a PV/CST hybrid system with an SBS film and a plot of the spectral irradiance of solar radiation and blackbody radiation.

Table 1. Deposition Parameters of the SiN_x/Cu SBS Film

		gas flow rate (sccm)		target power density (W/cm^2)			
layer	sputtering method	Ar	N_2	Cu	Si	deposition time (min)	operating pressure (Pa)
Cu	DC	22	0	5.48	0	1	0.9
SiN_x	RF	28	25	0	3.29	80	1.3

rate in the vacuum chamber. The solar SBS film composed of a 17 nm thick Cu layer and 67 nm thick SiN_x layer exhibited a maximum transmittance of 72.9% and a maximum reflectance of 89.7%. The XRD and EDS results confirmed the presence of Cu. The SiN_x/Cu SBS films became denser and showed fine Ag particles with uniform shapes and flat surfaces after annealing for different durations. The decreased rms roughness of the coatings led to decreased diffuse reflectance and increased transmittance. Thermal annealing studies indicated that the microstructure of the SiN_x/Cu solar SBS film evolved with increasing annealing time. However, no significant attenuation of the optical properties was observed after annealing for different durations. The coating annealed at 50 °C for 360 h exhibited a high transmittance of 71.8% and a reflectance of 88.5%. No diffusion of other atoms into the coating was observed. Thus, the SiN_x/Cu double-layer SBS film exhibits superior SBS properties and offers a new route for the development of PV/CST hybrid systems.

4. EXPERIMENTAL SECTION

4.1. Design. A novel double-layer SBS film of SiN_x/Cu was deposited on glass by magnetron sputtering. The thickness of the Cu film was set to ~10−20 nm. A thick film decreases the transmittance of light, whereas a thin film (less than 10 nm) causes severe light scattering. This is because the atoms in thin films diffuse and form islands or a discontinuous metal film.[32,33,36,37] The spectral splitting effect of the SBS film over a wider wavelength range was realized by superimposing a SiN_x film because it offers high transmittance in the wavelength range of 380−1100 nm and high reflectance in the rest of the solar wavelength range (300−2500 nm).

A PV/CST hybrid system with the SiN_x/Cu SBS film was developed based on the linear Fresnel solar thermal technology, as illustrated in Figure 11. The SiN_x/Cu SBS film was placed on the PV cell, which is referred to as the PV mirror. In this system, the SiN_x/Cu SBS film can transmit light in the range of 300−1100 nm to the PV cell and reflect the rest of the solar energy to the solar receiver tube with a compound parabolic concentrator reflector. The PV mirrors can track the path of the sun and reflect sunlight to the solar receiver tube. Owing to the optical performance of the SiN_x/Cu SBS film, the PV mirror can produce more power.

4.2. Deposition. The SiN_x/Cu SBS films were deposited on BK7 glass (dimensions: 76.2 mm × 25.4 mm) or Si substrates using a magnetron sputtering system (Kurt J. Lesker, USA). The films deposited on glass substrates were used for studying the optical properties, while those deposited on Si substrates were used for structural and morphological analyses. Before placing the substrates in the vacuum chamber, they were cleaned with alcohol and deionized water in an ultrasonic agitator to remove grease and dust from the surface. High-purity Cu and Si targets (99.99%, diameter: 76.2 mm) were used for the film deposition.

The targets were pre-sputtered with Ar gas for 30 min to clean the surface before the experiment. After achieving a base pressure of 5.5×10^{-6} Torr, Ar gas was introduced into the chamber. The target current and voltage were stabilized, and the substrate shield was opened before starting the deposition. The Cu layer was deposited via non-reactive sputtering of the Cu target in an Ar atmosphere (22 sccm). The SiN_x layer was deposited by reactive sputtering of the Si target in a mixed gas atmosphere (Ar: 28 sccm; N_2: 25 sccm). The substrate was rotated to improve the uniformity of the film during sputtering.

https://doi.org/10.1021/acsomega.1c03178
ACS Omega 2021, 6, 21709−21718

Single-layer Cu and SiN_x were deposited on BK7 glass substrates to study their optical properties, including the transmittance, reflectance, and cutoff wavelength. By optimizing the Ar flow rate, sputtering power, and sputtering time, a Cu layer with a high transmittance in the visible range and a high reflectance in the IR range was obtained. To optimize the solar selectivity of the SBS film, a SiN_x layer was deposited on the optimized Cu layer by adjusting the N_2 flow rate, in addition to the other parameters. The optimized deposition parameters are presented in Table 1. Finally, a novel spectral splitting coating of SiN_x/Cu was deposited on the BK7 glass substrate. The Cu and SiN_x layers were deposited on BK7 glass substrates for different times at the same Ar flow rate and sputtering power to study the effect of the layer thickness on the transmittance and reflectance.

To study the thermal stability, the coatings were annealed at 50 °C in an incubator for different durations ranging from 10 to 360 h. The accuracy of the set temperature was ±0.2 °C. The structural and optical properties of the annealed films were evaluated after the films were cooled to ambient temperature.

4.3. Characterization. The reflection and transmission spectra of the SiN_x/Cu SBS films in the solar spectral range (300−2500 nm) were obtained using a Cary 7000 UV/Vis/NIR spectrophotometer equipped with an integrating sphere (module 150 mm). The reflectance (ρ) and transmittance (τ) were calculated using eqs 1 and 2, respectively,

$$\rho = \frac{\int_{0.3\mu m}^{0.38\mu m} \rho(\theta, \lambda) I_S(\lambda) d\lambda + \int_{1.1\mu m}^{2.5\mu m} \rho(\theta, \lambda) I_S(\lambda) d\lambda}{\int_{0.3\mu m}^{0.38\mu m} I_S(\lambda) d\lambda + \int_{1.1\mu m}^{2.5\mu m} I_S(\lambda) d\lambda} \quad (1)$$

$$\tau = \frac{\int_{0.38\mu m}^{1.1\mu m} \tau(\theta, \lambda) I_S(\lambda) d\lambda}{\int_{0.38\mu m}^{1.1\mu m} I_S(\lambda) d\lambda} \quad (2)$$

where λ, $\rho(\theta,\lambda)$, $\tau(\theta,\lambda)$, and $I_S(\lambda)$ are the wavelength, the reflectance at a certain wavelength, the transmittance at a certain wavelength, and the direct normal solar irradiance, respectively, as defined according to ISO standard 9845-1 for normal radiance and an air mass of 1.5. ρ and τ are equally weighted fractions.

The surface features and fracture structure topography were studied by SEM (FV1000, Japan). EDS profiles of selected areas were recorded using an EDS instrument (FV1000, Japan). The surface morphology and roughness of the SBS coatings were investigated by AFM (ICON2-SYS Bruker Nano Inc). The crystal structures of the as-deposited and annealed samples were studied by XRD (D8-Focus, Bruker AXS, Germany).

AUTHOR INFORMATION

Corresponding Author

Dongqiang Lei − *Key Laboratory of Concentrating Solar Thermal Energy and Photovoltaic System, Chinese Academy of Sciences, Beijing 100190, China; Institute of Electrical Engineering, Chinese Academy of Sciences, Beijing 100190, China; University of Chinese Academy of Sciences, Beijing 100049, China; Beijing Engineering Research Center of Concentrating Solar Thermal Power, Beijing 100190, China*; Phone: +86-132-4045-8306; Email: ldqljmei@126.com

Authors

Xin Zhang − *Key Laboratory of Concentrating Solar Thermal Energy and Photovoltaic System, Chinese Academy of Sciences, Beijing 100190, China; Institute of Electrical Engineering, Chinese Academy of Sciences, Beijing 100190, China; University of Chinese Academy of Sciences, Beijing 100049, China; Beijing Engineering Research Center of Concentrating Solar Thermal Power, Beijing 100190, China*; orcid.org/0000-0003-0668-8400

Bo Zhang − *North University of China, Taiyuan, Shanxi 030051, China*

Pan Yao − *Key Laboratory of Concentrating Solar Thermal Energy and Photovoltaic System, Chinese Academy of Sciences, Beijing 100190, China; Institute of Electrical Engineering, Chinese Academy of Sciences, Beijing 100190, China; University of Chinese Academy of Sciences, Beijing 100049, China; Beijing Engineering Research Center of Concentrating Solar Thermal Power, Beijing 100190, China*

Zhifeng Wang − *Key Laboratory of Concentrating Solar Thermal Energy and Photovoltaic System, Chinese Academy of Sciences, Beijing 100190, China; Institute of Electrical Engineering, Chinese Academy of Sciences, Beijing 100190, China; University of Chinese Academy of Sciences, Beijing 100049, China; Beijing Engineering Research Center of Concentrating Solar Thermal Power, Beijing 100190, China*

Complete contact information is available at: https://pubs.acs.org/10.1021/acsomega.1c03178

Notes

The authors declare no competing financial interest.

ACKNOWLEDGMENTS

This work was funded by the National Key R&D Program of China (no. 2019YFE0102000).

REFERENCES

(1) Zhao, N.; Fengqi, Y. Can Renewable Generation, Energy Storage and Energy Efficient Technologies Enable Carbon Neutral Energy Transition? *Appl. Energy* **2020**, *279*, 115889.

(2) Liang, H.; Wang, F.; Cheng, Z.; Xu, C.; Li, G.; Shuai, Y. Full Spectrum Solar Energy Utilization and Enhanced Solar Energy__-harvesting via Antireflection and Scattering Performance Using Biomimetic Nanophotonic Structure. *ES Energy Environ.* **2020**, *8*, 29−41.

(3) Kumar, L.; Hasanuzzaman, M.; Rahim, N. A. Global Advancement of Solar Thermal Energy Technologies for Industrial Process Heat and Its Future Prospects: A Review. *Energy Convers. Manage.* **2019**, *195*, 885−908.

(4) Hjerrild, N. E.; Scott, J. A.; Amal, R.; Taylor, R. A. Exploring the effects of heat and UV exposure on glycerol-based Ag-SiO2 nanofluids for PV/T applications. *Renewable Energy* **2018**, *120*, 266−274.

(5) Yazdanifard, F.; Ameri, M. Exergetic Advancement of Photovoltaic/Thermal Systems (PV/T): A Review. *Renewable Sustainable Energy Rev.* **2018**, *97*, 529−553.

(6) Wang, G.; Yao, Y.; Wang, B.; Hu, P. Design and Thermodynamic Analysis of an Innovative Hybrid Solar PV-CT System with Multi-Segment PV Panels. *Sustain. Energy Technol. Assess.* **2020**, *37*, 100631.

(7) Widyolar, B.; Lun, J.; Jfa, B.; Rwa, B.; Ak, C.; Mo, C.; Dc, D.; Ha, D. Theoretical and Experimental Performance of a Two-Stage (50X) Hybrid Spectrum Splitting Solar Collector Tested to 600°C. *Appl. Energy* **2019**, *239*, 514−525.

(8) Zhang, G.; Wei, J.; Xie, H.; Wang, Z.; Xi, Y.; Khalid, M. Performance Investigation on a Novel Spectral Splitting Concentrat-

ing Photovoltaic/Thermal System Based on Direct Absorption Collection. *Sol. Energy* **2018**, *163*, 552−563.
(9) Huang, G.; Curt, S. R.; Wang, K.; Markides, C. N. Challenges and Opportunities for Nanomaterials in Spectral Splitting for High-Performance Hybrid Solar Photovoltaic-Thermal Applications: A Review. *Nano Mater. Sci.* **2020**, *2*, 183−203.
(10) Wang, G.; Yao, Y.; Lin, J.; Chen, Z.; Hu, P. Design and Thermodynamic Analysis of a Novel Solar CPV and Thermal Combined System Utilizing Spectral Beam Splitter. *Renewable Energy* **2020**, *155*, 1091−1102.
(11) Wei, D.; Cao, F.; Wu, Z.; Liu, Y.; Wang, J.; Wang, Q.; Liu, X.; Zhang, Q. Enhanced Spectral Splitting in a Novel Solar Spectrum Optical Splitter Based on One Dimensional Photonic Crystal Heterostructure. *J. Materiomics* **2021**, *7*, 648−655.
(12) Liang, H.; Han, H.; Wang, F.; Cheng, Z.; Lin, B.; Pan, Y.; Tan, J. Experimental Investigation on Spectral Splitting of Photovoltaic/Thermal Hybrid System with Two-Axis Sun Tracking Based on SiO2/TiO2 Interference Thin Film. *Energy Convers. Manage.* **2019**, *188*, 230−240.
(13) Wang, G.; Yao, Y.; Chen, Z.; Hu, P. Thermodynamic and Optical Analyses of a Hybrid Solar CPV/T System with High Solar Concentrating Uniformity Based on Spectral Beam Splitting Technology. *Energy* **2019**, *166*, 256−266.
(14) Imenes, A. G.; Buie, D.; McKenzie, D. The Design of Broadband, Wide-Angle__interference Filters for Solar Concentrating Systems. *Sol. Energy Mater. Sol. Cells* **2006**, *90*, 1579.
(15) Jiang, S.; Hu, P.; Mo, S.; Chen, Z. Optical Modeling for a Two-Stage Parabolic Trough Concentrating Photovoltaic/Thermal System Using Spectral Beam Splitting Technology. *Sol. Energy Mater. Sol. Cells* **2010**, *94*, 1686−1696.
(16) Jiang, S.-L.; Peng, H.; Mo, S. P.; Chen, Z.-s. *Modeling for Two-Stage Dish Concentrating Spectral Beam Splitting/Photovoltaic_thermal System*; IEEE, 2009.
(17) Eisler, C.; Flowers, C.; Warmann, E.; Lloyd, J.; Espinet-González, P.; Darbe, S.; Dee, M.; Escarra, M.; Kosten, E.; Zhou, W.; Atwater, H. The Polyhedral Specular Reflector: A Spectrum-Splitting Multijunction Design to Achieve Ultrahigh (>50%) Solar Module Efficiencies. *IEEE J. Photovolt.* **2018**, *9*, 174−182.
(18) Wang, G.; Wang, B.; Yao, Y.; Lin, J.; Chen, Z.; Hu, P. Parametric Study on Thermodynamic Performance of a Novel PV Panel and Thermal Hybrid Solar System. *Appl. Therm. Eng.* **2020**, *180*, 115807.
(19) Crisostomo, F.; Taylor, R. A.; Zhang, T.; Perez-Wurfl, I.; Rosengarten, G.; Everett, V.; Hawkes, E. R. Experimental testing of SiN x /SiO 2 thin film filters for a concentrating solar hybrid PV/T collector. *Renewable Energy* **2014**, *72*, 79−87.
(20) Sibin, K. P.; Selvakumar, N.; Kumar, A.; Dey, A.; Sridhara, N.; Shashikala, H. D.; Sharma, A. K.; Barshilia, H. C. Design and Development of ITO/Ag/ITO Spectral Beam Splitter Coating for Photovoltaic-Thermoelectric Hybrid Systems. *Sol. Energy* **2017**, *141*, 118−126.
(21) Wang, L.; Shen, Z.; Du, G.; Wang, P.; Wang, P. The Thermal Stability of Silver-Based High Reflectance Coatings. *Thin Solid Films* **2016**, *616*, 122−125.
(22) Li, F.; Zhang, Y.; Wu, C.; Lin, Z.; Zhang, B.; Guo, T. Improving Efficiency of Organic Light-Emitting Diodes Fabricated Utilizing AZO/Ag/AZO Multilayer Electrode. *Vacuum* **2012**, *86*, 1895−1897.
(23) Zhu, B. L.; Ma, J. M.; Lv, K.; Wang, C. J.; Wu, J.; Gan, Z. H.; Liu, J.; Shi, X. W. Improvement of Transparent Conductive Properties of GZO/Cu/GZO Tri-Layer Films by Introducing H_2 into Sputtering Atmosphere. *Superlattices Microstruct.* **2020**, *140*, 106456.
(24) Du, M.; Lei, H.; Jing, M.; Fang, L.; Liu, X.; Jiang, L.; Wang, S. Optimization Design of Ti0.5Al0.5N/Ti0.25Al0.75N/AlN Coating Used for Solar Selective Applications. *Sol. Energy Mater. Sol. Cells* **2011**, *95*, 1193−1196.
(25) Guo, H.-X.; Yu, D.-M.; He, C.-Y.; Qiu, X.-L.; Zhao, S.-S.; Liu, G.; Gao, X.-H. Double-Layer Solar Absorber Coating Based on High Entropy Ceramic AlCrMoTaTiN: Structure, Optical Properties and Failure Mechanism. *Surf. Interfaces* **2021**, *24*, 101062.
(26) Cao, F.; Tang, L.; Li, Y.; Litvinchuk, A. P.; Bao, J.; Ren, Z. A High-Temperature Stable Spectrally-Selective Solar Absorber Based on Cermet of Titanium Nitride in SiO2 Deposited on Lanthanum Aluminate. *Sol. Energy Mater. Sol. Cells* **2017**, *160*, 12−17.
(27) Liu, Y.; Wang, Z.; Lei, D.; Wang, C. A new solar spectral selective absorbing coating of SS-(Fe3O4)/Mo/TiZrN/TiZrON/SiON for high temperature application. *Sol. Energy Mater. Sol. Cells* **2014**, *127*, 143−146.
(28) He, C.-Y.; Gao, X.-H.; Yu, D.-M.; Qiu, X.-L.; Guo, H.-X.; Liu, G. Scalable and Highly Efficient High Temperature Solar Absorber Coatings Based on High Entropy Alloy Nitride AlCrTaTiZrN with Different Antireflection Layers. *J. Mater. Chem. A* **2021**, *9*, 6413.
(29) Mardiansyah, D.; Trevon, B.; Kuwat, T.; Mehmood, M. Q.; Niloufar, R. H.; Yoonkyung, L.; Harsojo, S.; Kyunghoon, K.; Junsuk, R. Effect of Temperature on the Oxidation of Cu Nanowires and Development of an Easy to Produce, Oxidation-Resistant Transparent Conducting Electrode Using a PEDOT:PSS Coating. *Sci. Rep.* **2018**, *8*, 10639.
(30) He, Q.; Tian, Y.; Wu, Y.; Liu, J.; Li, G.; Deng, P.; Chen, D. Electrochemical Sensor for Rapid and Sensitive Detection of Tryptophan by a Cu2O Nanoparticles-Coated Reduced Graphene Oxide Nanocomposite. *Biomolecules* **2019**, *9*, 176.
(31) Tan, J.; Dun, M.; Li, L.; Zhao, J.; Li, X.; Hu, Y.; Huang, G.; Tan, W.; Huang, X. Self-Template Derived CuO Nanowires Assembled Microspheres and Its Gas Sensing Properties. *Sens. Actuators, B* **2017**, *252*, 1−8.
(32) Bernède, J. C.; Cattin, L.; Abachi, T.; Lare, Y.; Morsli, M.; Makha, M. Use of Cu-Ag Bi-Layer Films in Oxide/Metal/Oxide Transparent Electrodes to Widen Their Spectra of Transmittance. *Mater. Lett.* **2013**, *112*, 187−189.
(33) Li, S.-s.; Wang, Y.-l.; Li, B.-j.; Huang, L.-j.; Ren, N.-f. Femtosecond Laser Selective Ablation of Cu/Ag Double-Layer Metal Films for Fabricating High-Performance Mesh-Type Transparent Conductive Electrodes and Heaters. *Opt. Commun.* **2021**, *483*, 126661.
(34) Micheli, L.; Fernández, E. F.; Almonacid, F.; Mallick, T. K.; Smestad, G. P. Performance, Limits and Economic Perspectives for Passive Cooling of High Concentrator Photovoltaics. *Sol. Energy Mater. Sol. Cells* **2016**, *153*, 164−178.
(35) Gao, X.-H.; Wang, C.-B.; Guo, Z.-M.; Geng, Q.-F.; Theiss, W.; Liu, G. Structure, Optical Properties and Thermal Stability of Al2O3-WC Nanocomposite Ceramic Spectrally Selective Solar Absorbers. *Opt. Mater.* **2016**, *58*, 219−225.
(36) Zhou, H.; Xie, J.; Mai, M.; Wang, J.; Shen, X.; Wang, S.; Zhang, L.; Kisslinger, K.; Wang, H.-Q.; Zhang, J.; Li, Y.; Deng, J.; Ke, S.; Zeng, X. High-Quality AZO/Au/AZO Sandwich Film with Ultralow Optical Loss and Resistivity for Transparent Flexible Electrodes. *ACS Appl. Mater. Interfaces* **2018**, *10*, 16160−16168.
(37) Wang, M.; Choy, K.-L. All-Nonvacuum-Processed CIGS Solar Cells Using Scalable Ag NWs/AZO-Based Transparent Electrodes. *ACS Appl. Mater. Interfaces* **2016**, *8*, 16640−16648.

https://doi.org/10.1021/acsomega.1c03178
ACS Omega 2021, 6, 21709−21718